Supporting Information for

Solar Hydrogen Production using Molecular Catalysts Immobilized on Gallium Phosphide (111)A and (111)B Polymer-Modified Photocathodes

Anna M. Beiler, Diana Khusnutdinova, Samuel I. Jacob and Gary F. Moore*

School of Molecular Sciences and the Biodesign Institute Center for Applied Structural Discovery (CASD), Arizona State University, Tempe, AZ 85287-1604, United States

gfmoore@asu.edu

Index

1. **Optical Characterization of Materials** S2
2. **FTIR data** S3
3. **NMR spectra** S5
4. **XPS data** S6
5. **PVI Film Thickness Determination via Ellipsometry** S15
6. **Electrochemical and Photoelectrochemical Data** S16
7. **Spectral Output of Lamp** S20
8. **Table of N 1s Peaks** S21
9. **Supplemental Information References** S22

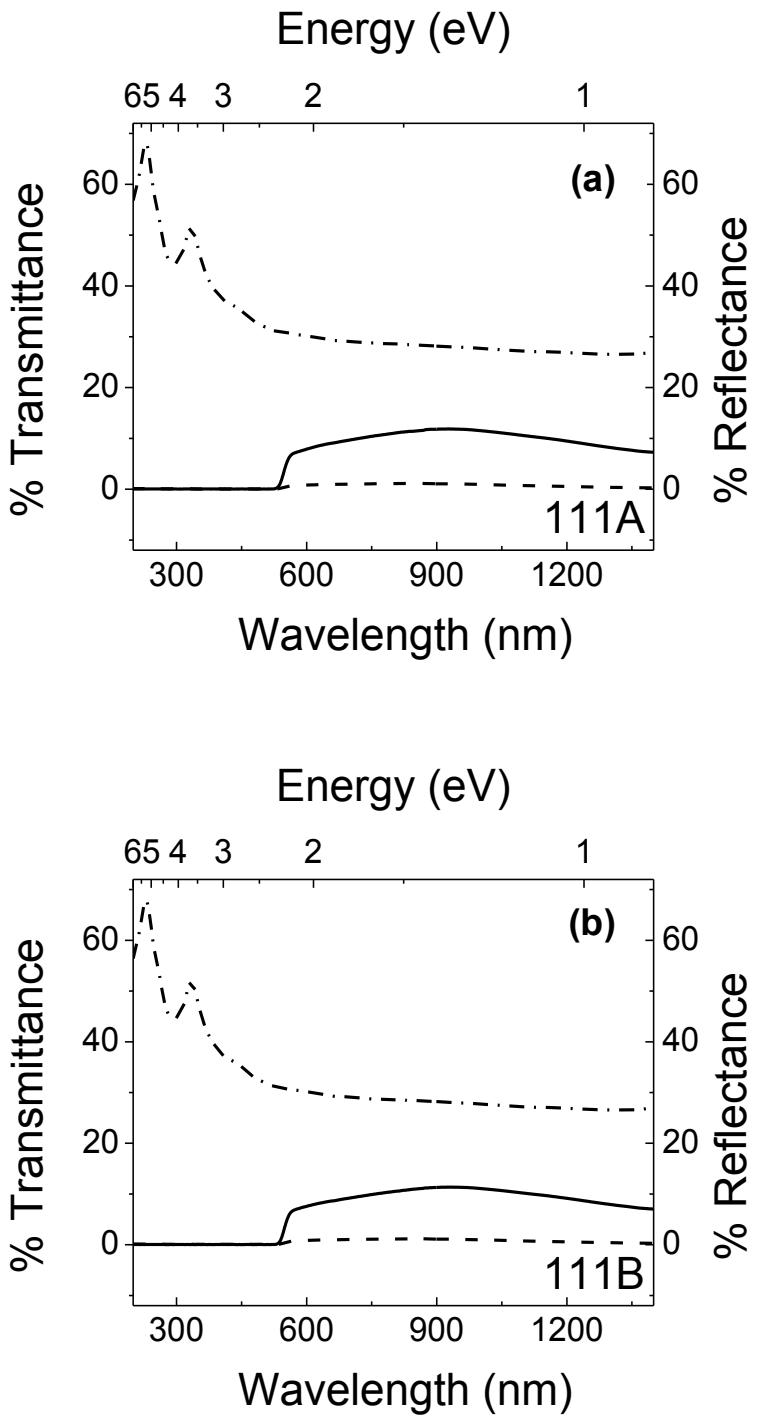

Figure S1. The transmission spectrum (solid line) as well as the relative specular reflectance (dashed-dotted) and diffuse reflectance (dashed) spectra for **(a)** GaP(111)A and **(b)** GaP(111)B.

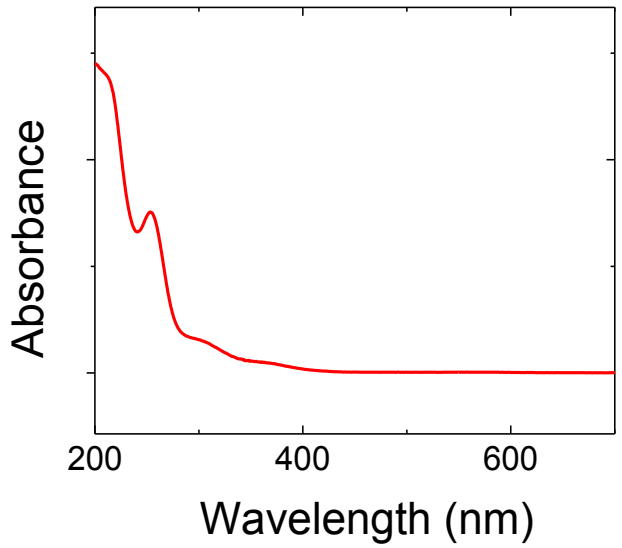

Figure S2. Absorbance spectrum of model compound, $Co(dmgH)_2(meIm)Cl$, recorded in acetonitrile.

FTIR data

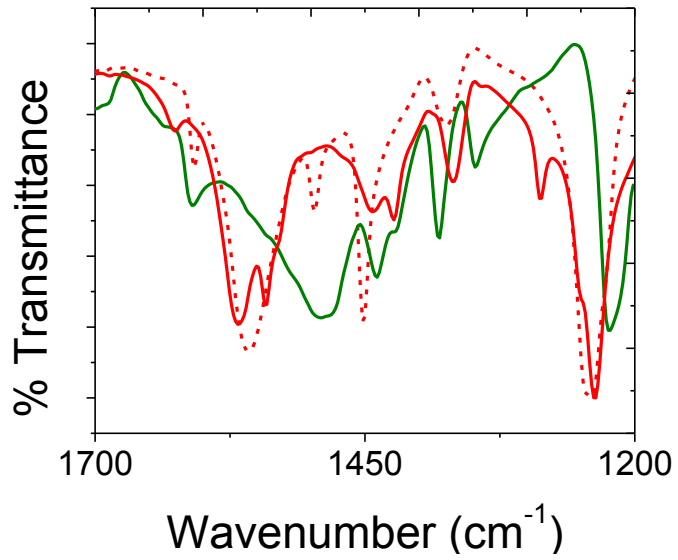

Figure S3. FTIR transmission spectra of $Co(dmgH_2)(dmgH)Cl_2$ (green), $Co(dmgH)_2(Py)Cl$ (dashed dark red) and $Co(dmgH)_2(meIm)Cl$ (red) in KBr.

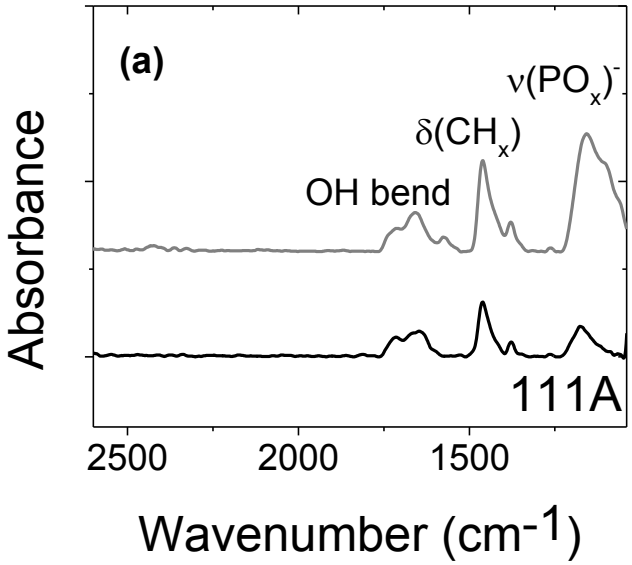

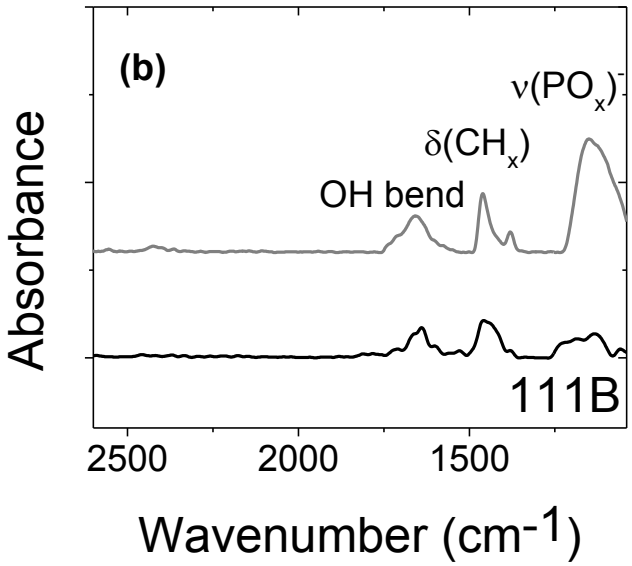

Figure S4. GATR-FTIR spectra of unmodified **(a)** GaP(111)A and**(b)** GaP(111)B before (gray) and after (black) etching with H_2SO_4.

NMR data

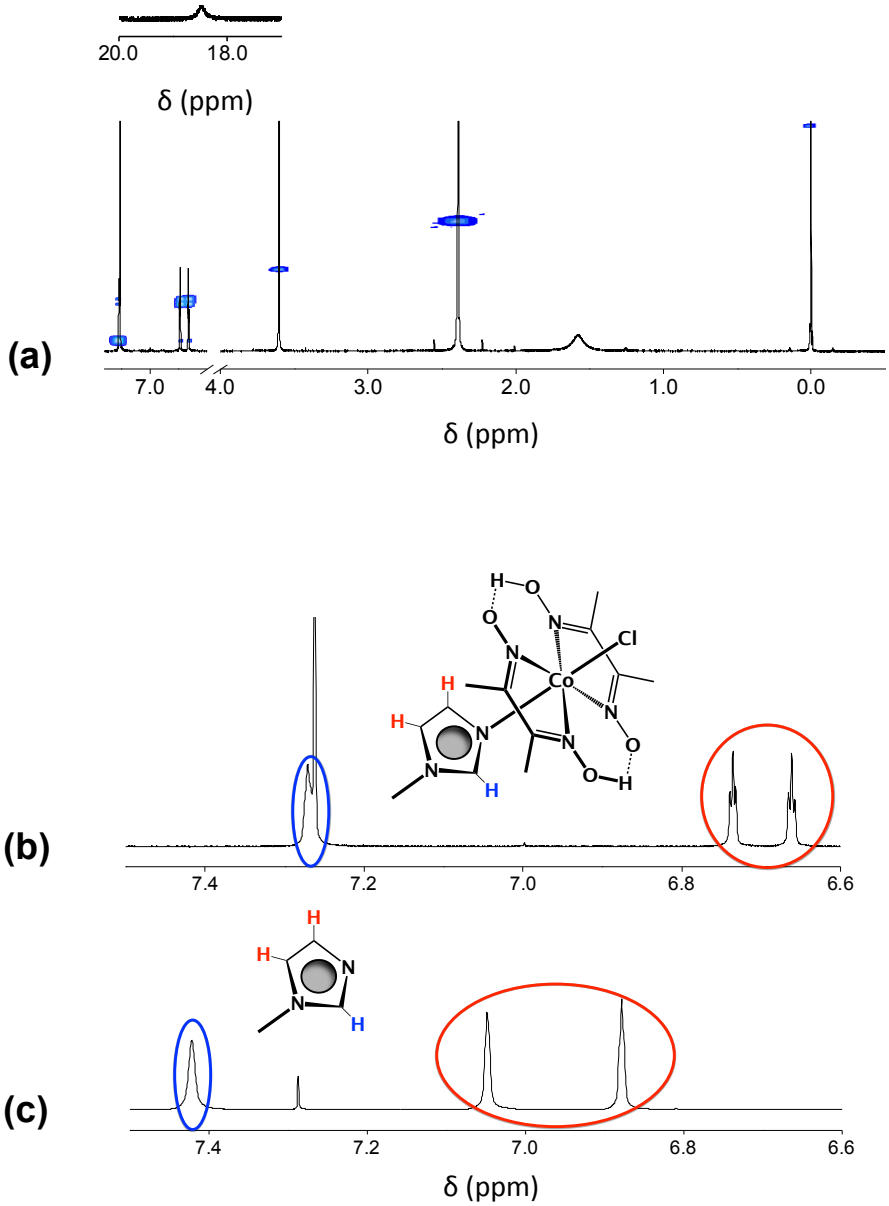

Figure S5. ^{1}H NMR spectra (black) with overlaid COSY (blue) of $Co(dmgH)_2(meIm)Cl$ in chloroform-d showing (**a**) features from 0 ppm to 7.25 ppm associated with the single aliphatic methyl resonance of the dimethylglyoximate ligands and aromatic resonances of the imidazole ligand and (**a, inset**) the single OH proton resonance of the dimethylglyoximate ligands at 18.5 ppm as well as (**b**) features at 6.6 ppm to 7.5 ppm associated with the aromatic resonances of the imidazole ligand. The methylimidazole ligand aromatic resonances from 6.6 to 7.5 ppm are shown in (**c**) for comparison.

XPS data

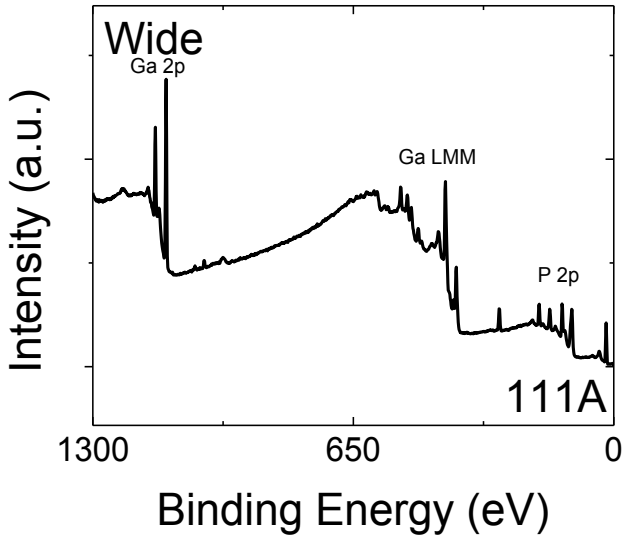

Figure S6: XP survey spectrum of unmodified GaP(111)A.

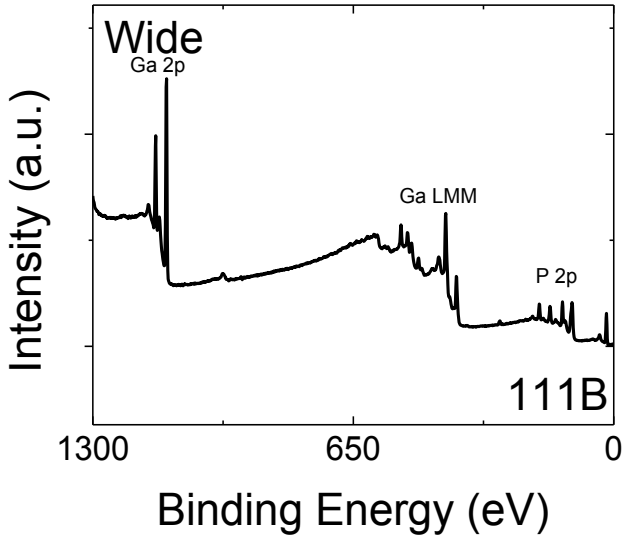

Figure S7: XP survey spectrum of unmodified GaP(111)B.

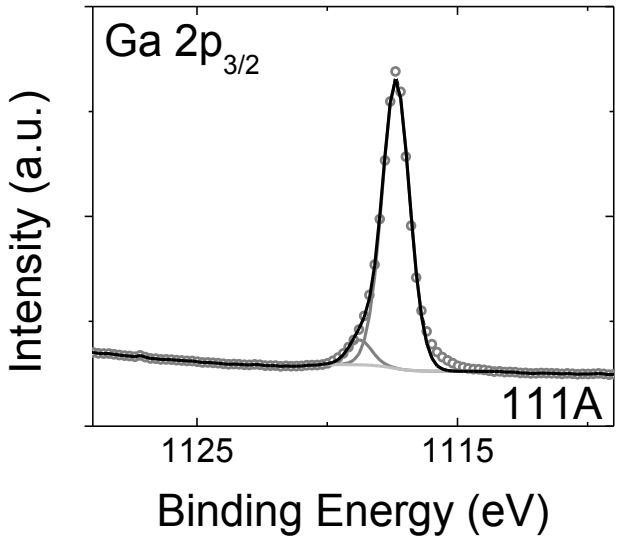

Figure S8: XP spectrum of the Ga $2p_{3/2}$ region of unmodified GaP(111)A. The circles are the spectral data, and the solid lines represent the background (light gray), component fit (dark gray), and overall fit (black). The Ga $2p_{3/2}$ spectral intensity ratio, A_{Ga-O}/A_{Ga-P}, is 0.08.

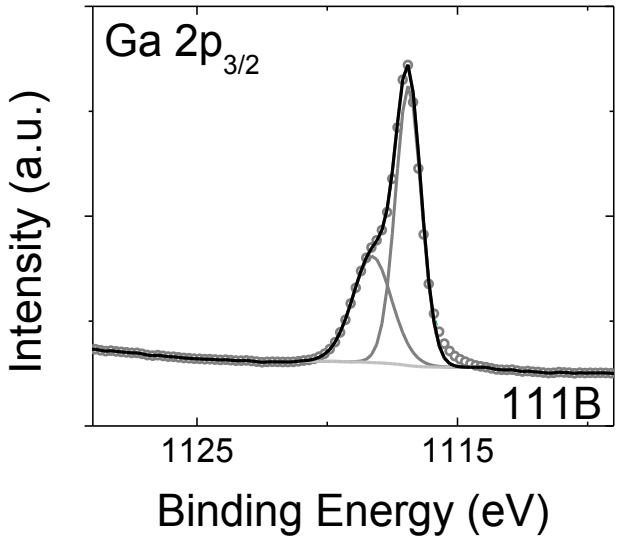

Figure S9: XP spectrum of the Ga $2p_{3/2}$ region of unmodified GaP(111)B. The circles are the spectral data, and the solid lines represent the background (light gray), component fit (dark gray), and overall fit (black). The Ga $2p_{3/2}$ spectral intensity ratio, A_{Ga-O}/A_{Ga-P}, is 0.49.

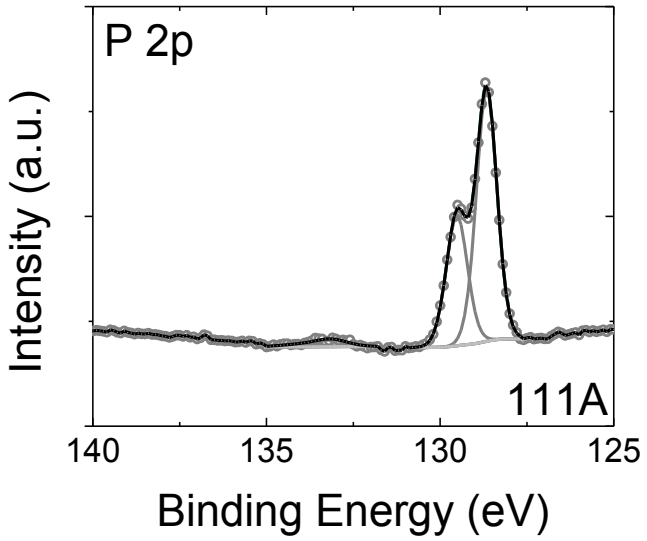

Figure S10: XP spectrum of the P 2p region of unmodified GaP(111)A. The circles are the spectral data, and the solid lines represent the background (light gray), component fit (dark gray), and overall fit (black). The P 2p spectral intensity ratio, A_{P-O}/A_{P-Ga}, is 0.04.

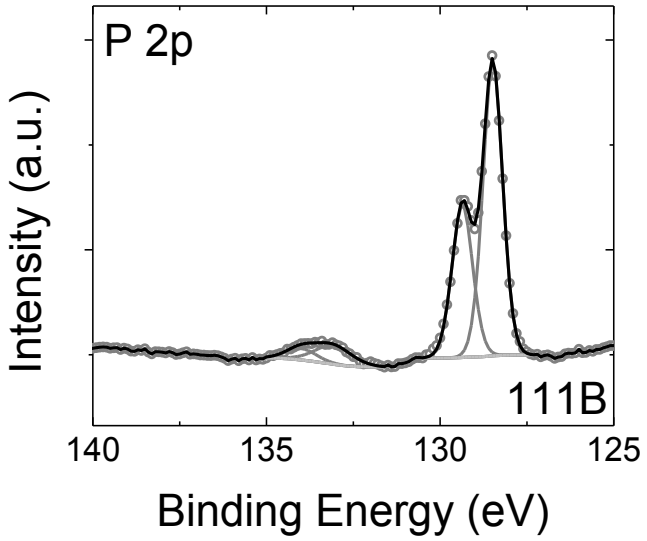

Figure S11: XP spectrum of the P 2p region of unmodified GaP(111)B. The circles are the spectral data, and the solid lines represent the background (light gray), component fit (dark gray), and overall fit (black). The P 2p spectral intensity ratio, A_{P-O}/A_{P-Ga}, is 0.12.

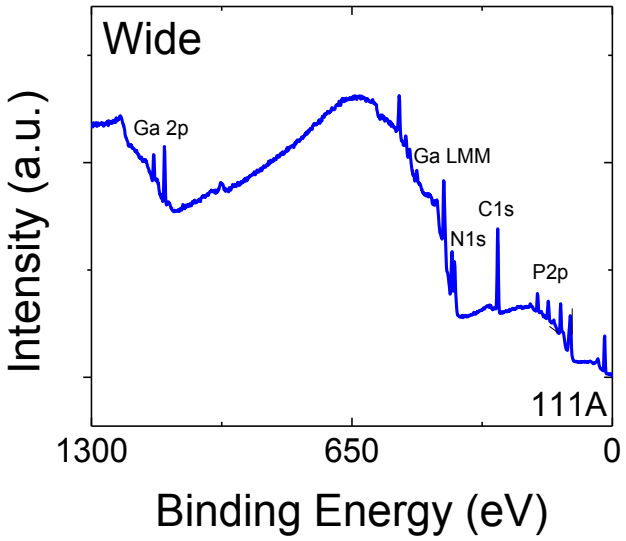

Figure S12: XP survey spectrum of PVI-GaP(111)A.

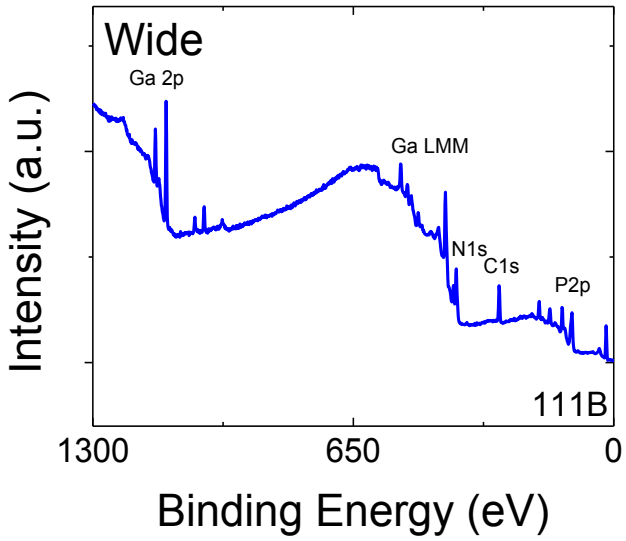

Figure S13: XP survey spectrum of PVI-GaP(111)B.

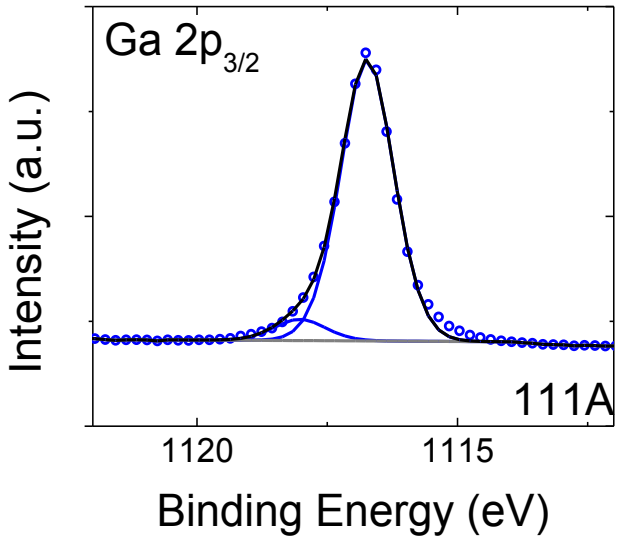

Figure S14: XP spectrum of the Ga $2p_{3/2}$ region of PVI-GaP(111)A. The circles are the spectral data, and the solid lines represent the background (light gray), component fit (blue), and overall fit (black).

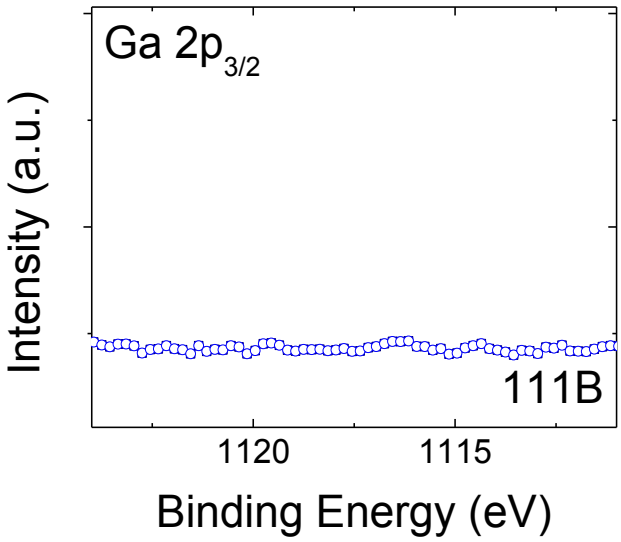

Figure S15: XP spectrum of the Ga $2p_{3/2}$ region of PVI-GaP(111)B. The circles are the spectral data.

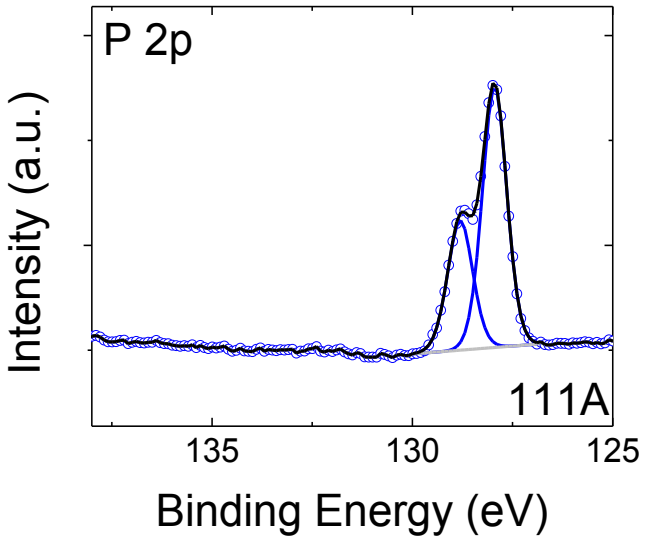

Figure S16: XP spectrum of the P 2p region of PVI-GaP(111)A. The circles are the spectral data, and the solid lines represent the background (light gray), component fit (blue), and overall fit (black).

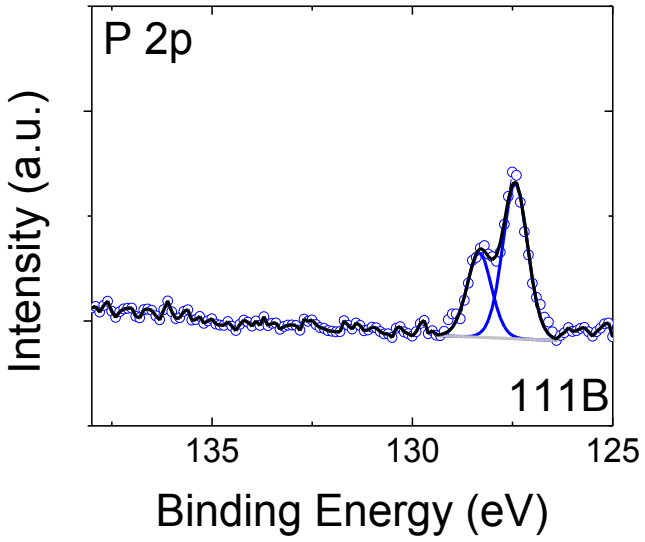

Figure S17: XP spectrum of the P 2p region of PVI-GaP(111)B. The circles are the spectral data, and the solid lines represent the background (light gray), component fit (blue), and overall fit (black).

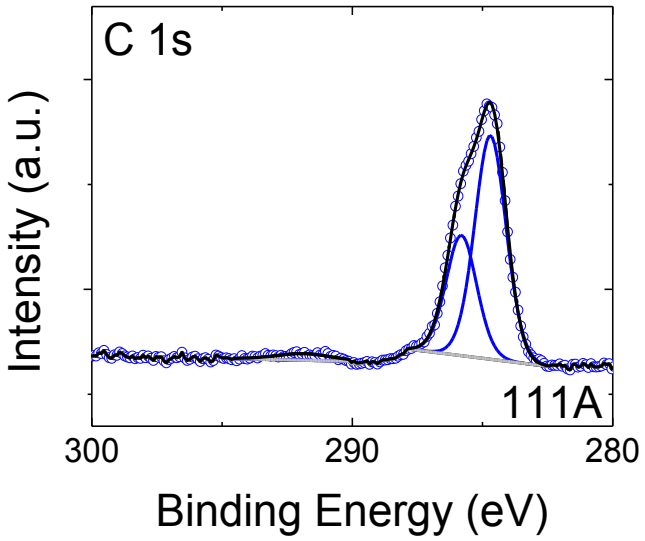

Figure S18. XP spectrum of the C 1s region of PVI-GaP(111)A. The circles are the spectral data, and the solid lines represent the background (light gray), component fit (blue), and overall fit (black).

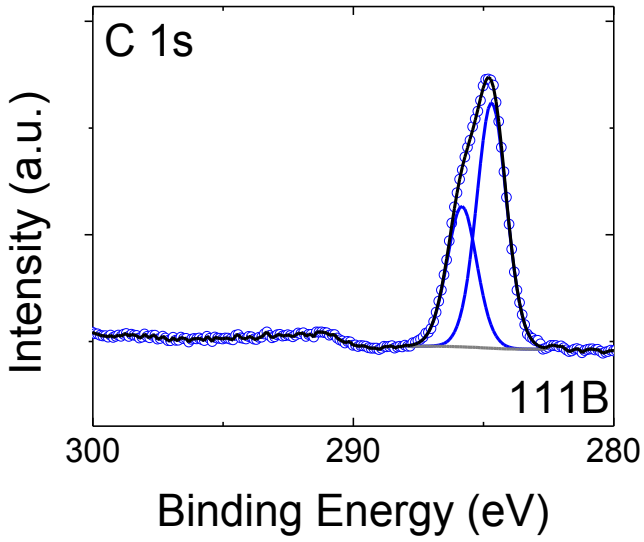

Figure S19. XP spectrum of the C 1s region of PVI-GaP(111)B. The circles are the spectral data, and the solid lines represent the background (light gray), component fit (blue), and overall fit (black).

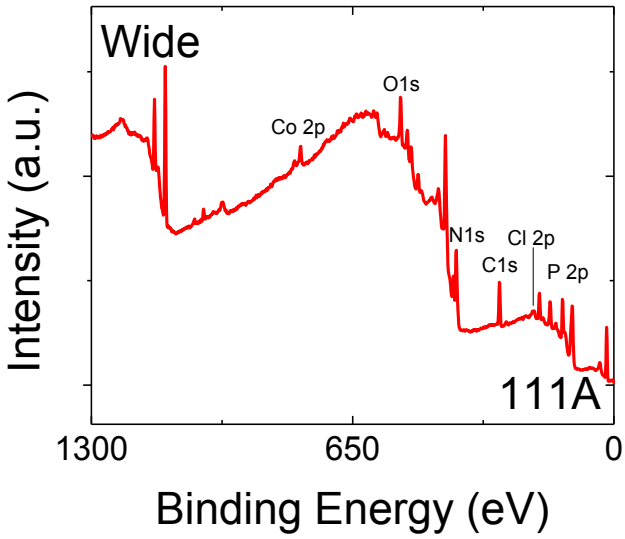

Figure S20: XP survey spectrum of Co-PVI-GaP(111)A.

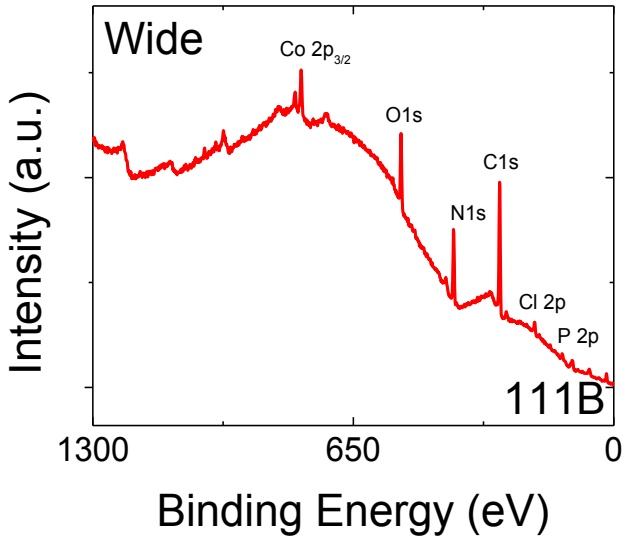

Figure S21: XP survey spectrum of Co-PVI-GaP(111)B.

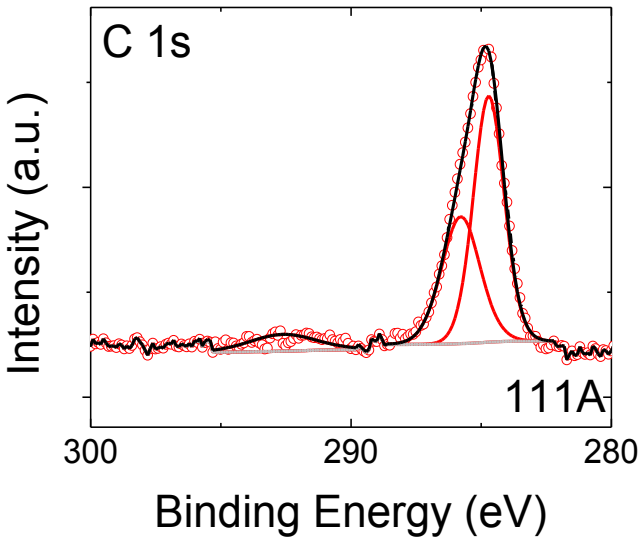

Figure S22: XP spectrum of the C 1s region of Co-PVI-GaP(111)A. The circles are the spectral data, and the solid lines represent the background (light gray), component fit (red), and overall fit (black).

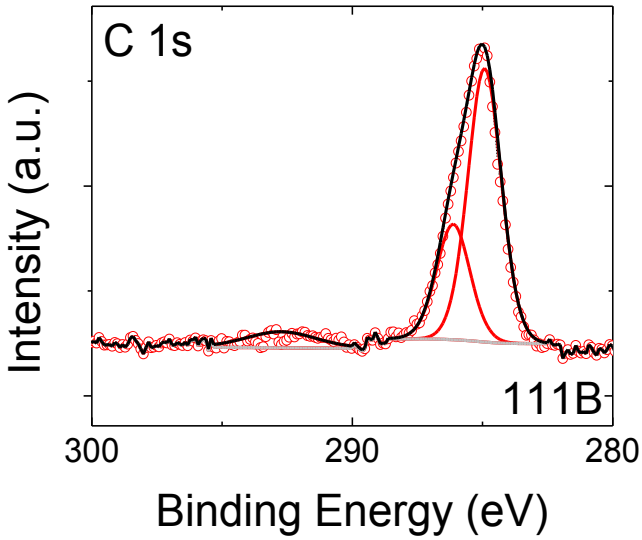

Figure S23: XP spectrum of the C 1s region of Co-PVI-GaP(111)B. The circles are the spectral data, and the solid lines represent the background (light gray), component fit (red), and overall fit (black).

Ellipsometry Data

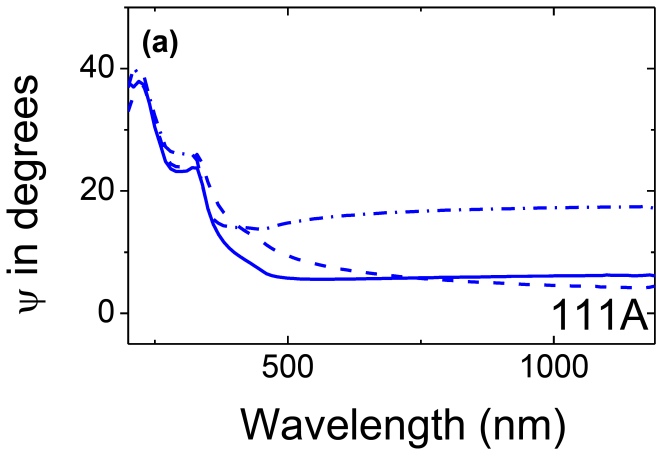

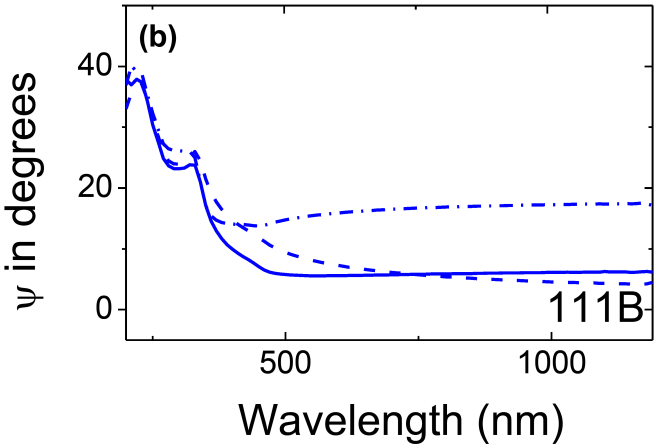

Figure S24. Ellipsometry spectra taken at 70° (dashed), 75° (solid), and 80° (dashed-dotted) of polyvinylimidazole-functionalized **(a)** GaP(111)A and **(b)** GaP(111)B.

Electrochemical and Photoelectrochemical Data

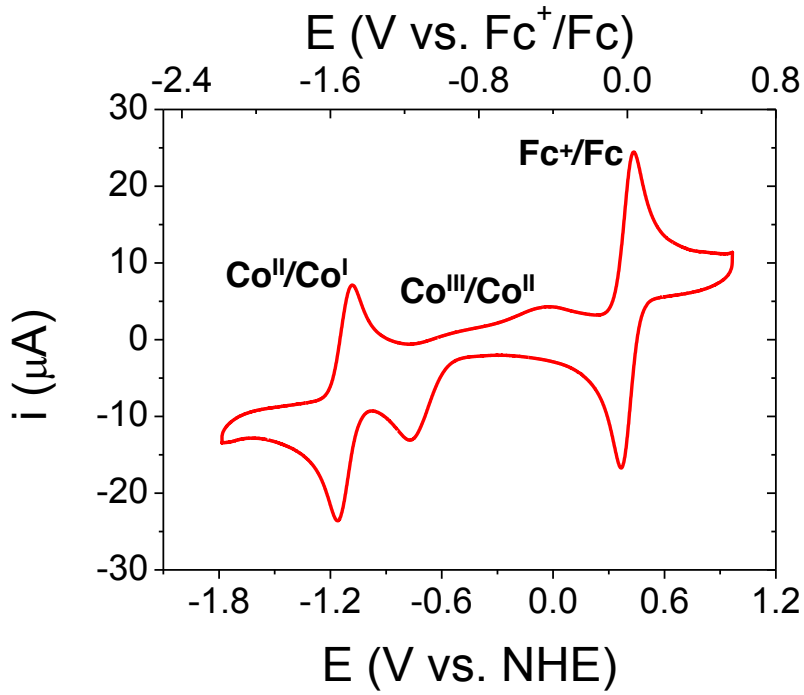

Figure S25. Cyclic voltammogram of $Co(dmgH)_2(meIm)Cl$ recorded in 0.1 M tetrabutylammonium hexafluorophosphate in acetonitrile at a scan rate of 100 mV s^{-1} with a glassy carbon working electrode at room temperature and ferrocene as an internal standard with $E_{1/2}$ taken as 0.40 V vs. NHE[1].

	$^{II}E_{1/2}$	$^{I}E_{1/2}$
$Co(dmgH)_2(meIm)Cl$	-1.52 V vs. Fc^+/Fc (ΔE_p = 75 mV)	-0.80 V vs. Fc^+/Fc (ΔE_p = 745 mV)

Table S1. Potentials for reduction (nE) of $Co(dmgH)_2(meIm)Cl$, as determined by cyclic voltammetry. Peak-to-peak separations of the observed redox couples (ΔE_p) are reported in parenthesis. The electrolyte was 0.1 M tetrabutylammonium hexafluorophosphate in acetonitrile, and the scan rate was 250 mV s^{-1}. The potential of the pseudoreference electrode was determined using the ferrocenium/ferrocene redox couple as an internal standard.

.

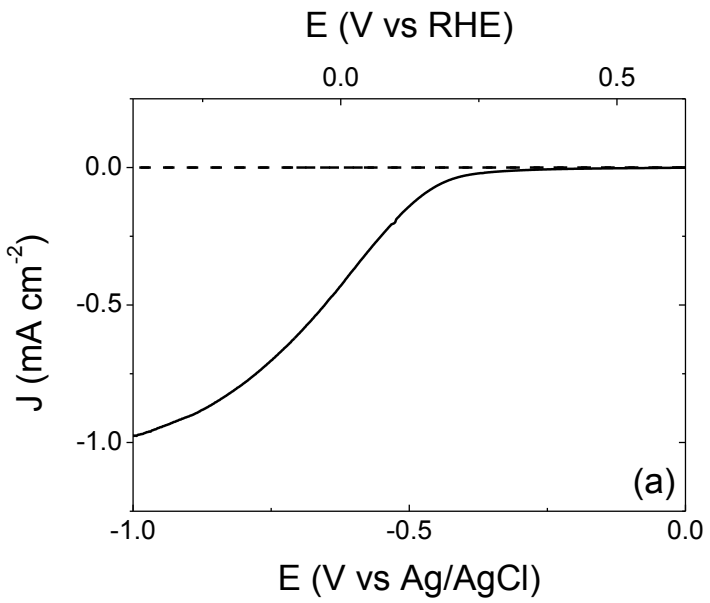

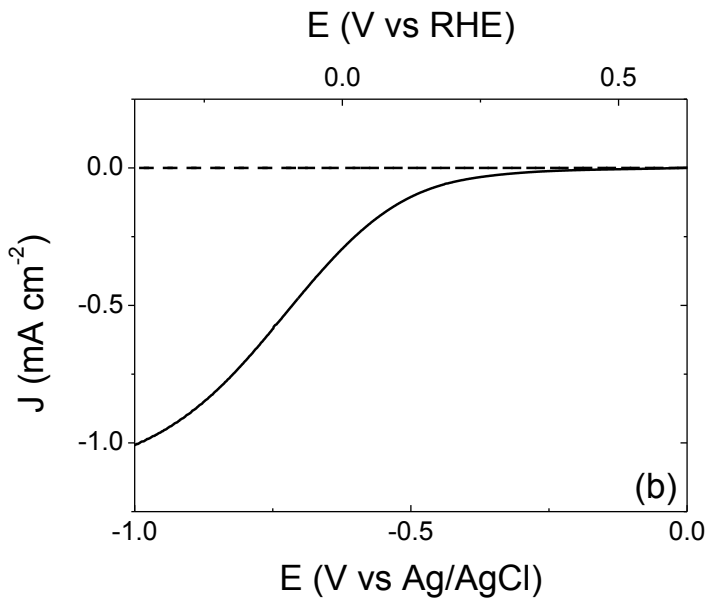

Figure S26: Linear sweep voltammograms of unmodified **(a)** GaP(111)A and **(b)** GaP(111)B in the dark (dashed lines) and under 100 mW cm^{-2} illumination in 0.1 M phosphate buffer (pH 7) with a 100 mV s^{-1} sweep rate.

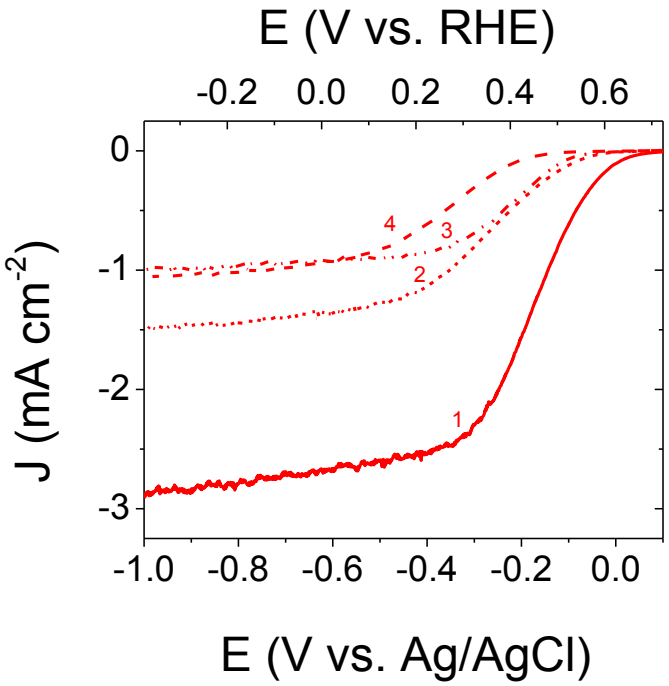

Figure S27. Linear sweep voltammograms of working electrodes using GaP substrates with the following properties and illumination conditions:

1 (solid line) illuminated with a Newport Oriel Apex illuminator (100 mW cm^{-2}) using cobaloxime-polyvinylpyridine-modified Zn doped p-GaP(100) with a resistivity of 1.17 x 10^{-1} Ω.cm, a mobility of 77 cm^2 V^{-1} s^{-1}, and a carrier concentration of 6.95 x 10^{17} cm^{-3}

2 (dotted line) illuminated with a Solar Light PV cell test simulator (100 mW cm^{-2}) using the same electrode described in 1

3 (dashed-dotted line) illuminated with a Solar Light PV cell test simulator (100 mW cm^{-2}) using cobaloxime-polyvinylpyridine-modified Zn doped p-GaP (100) with a resistivity of 5.5 x 10^{-2} Ω cm, a mobility of 54 cm^2 V^{-1} s^{-1} and a carrier concentration of 2.2 x 10^{18} cm^{-3}

4 (dashed line) illuminated with a LSC-100 Series Oriel Solar Simulator equipped with an AM 1.5 filter (100 mW cm^{-2}) using cobaloxime-polyvinylimidazole-modified Zn doped p-GaP(111)A with a resistivity of 4.6 x 10^{-2} Ω cm, a mobility of 50 cm^2 V^{-1} s^{-1} and a carrier concentration of 2.7 x 10^{18} cm^{-3}

These results show that the JV response of the functionalized electrodes depends on the physical properties of the semiconductor substrate as well as the illumination conditions.

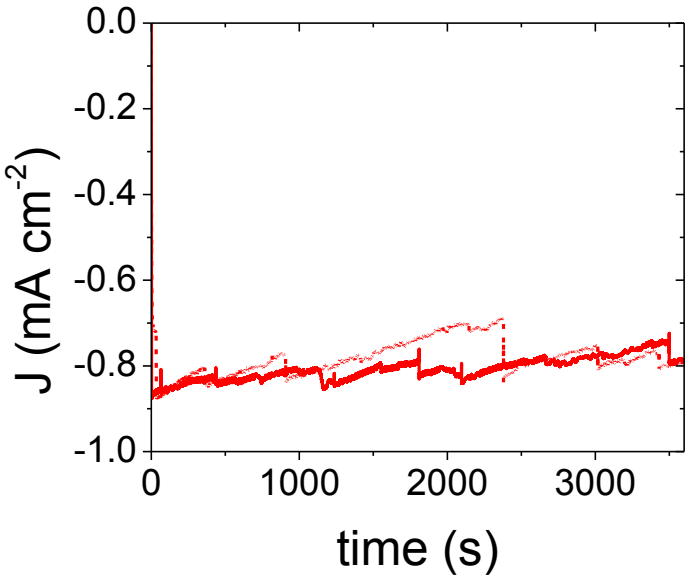

Figure S28. Three-electrode electrolysis measurements using cobaloxime-modified GaP(111)A (dashed) and cobaloxime-modified GaP(111)B (solid) working electrodes polarized at +0.01 V vs. RHE and under 1 sun illumination in phosphate buffer (pH 7). In these experiments, hydrogen bubbles, accumulating on the cobaloxime-modified photocathode surface during PEC operation, can inhibit diffusion of electrolyte to the photocathode and contribute a transient diminution of photocurrent as bubbles form and are removed at the working electrode surface.

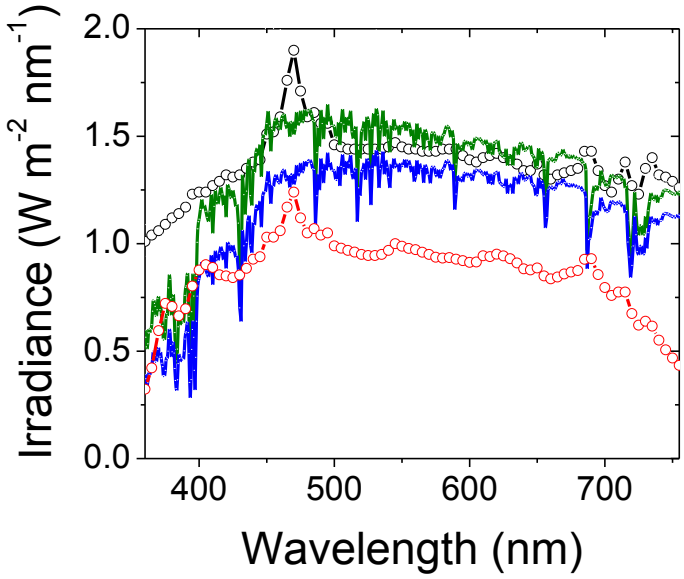

Figure S29. Spectral output of a LSC-100 Series Oriel Solar Simulator collected with (red circles) and without (black circles) an AM1.5 filter. For comparison, the air mass 1.5 global tilt (green) and direct circumsolar (blue) spectra are included.[2]

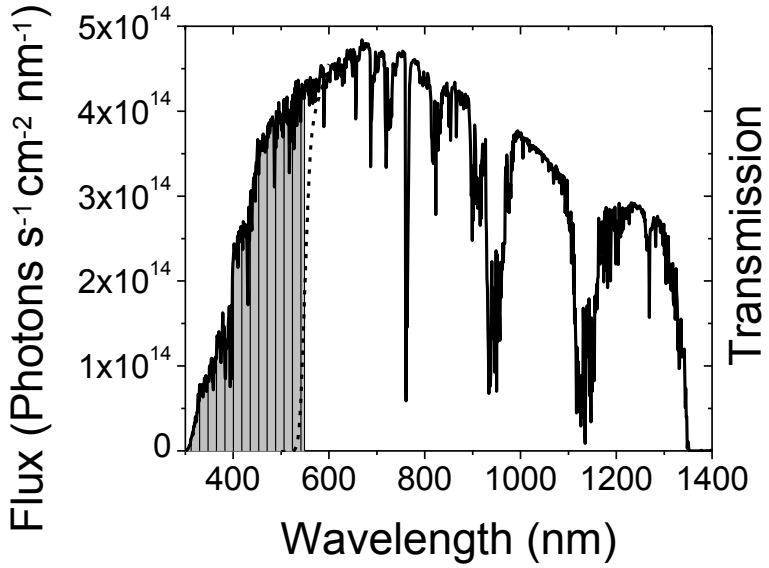

Figure S30. The air mass 1.5 global tilt solar flux spectrum (solid) and the transmission spectrum of the GaP substrates used in these experiments (dashed). The shaded grey area shows the integrated region of the solar spectrum from 280 nm up to the band gap of GaP (E_g = 2.26 eV = 549 nm), representing the theoretical maximum number of photons (6.0 x 10^{16} photons s^{-1} cm^{-2}) that can be collected. If all available photons give rise to current, the maximum theoretical photocurrent density is 9.6 mA cm^{-2}. However, actual photocurrent densities are always lower given reflection and transmission losses (Fig. 4) as well as other "parasitic" processes[3] that preclude absorbed photons from being converted to charge carriers moving through a potential. In addition, catalysts immobilized on a surface can also absorb a fraction of the incident photons.[4]

Table S2: N 1s Binding Energies (eV) for Figure 2

Construct	Imine nitrogen	Amine nitrogen	Co-imine nitrogen	Co-amine nitrogen	Glyoximate nitrogen
PVI-GaP(111)A	398.0	399.8	--	--	--
Co-PVI-GaP(111)A	398.5	399.6	399.6	400.7	400.4
PVI-GaP(111)B	398.2	400.1	--	--	--
Co-PVI-GaP(111)B	398.6	399.8	399.7	401.0	400.4

Supporting Information References

1) Koepp, H. M.; Wendt, H.; Stkehlow, H. Der Vergleich der Spannungsreihen in verschiedenen Solventien. II. *Zeitschrift für Elektrochemie, Berichte der Bunsengesellschaft für physikalische Chemie*. **1960**, *64,* 483–491. doi:10.1002/bbpc.19600640406
2) At the time of writing, the air-mass 1.5 global tilt (AM 1.5G) and direct circumsolar (AM 1.5D) solar spectra, from the ASTM G173-03 data set, is available online at http://rredc.nrel.gov/solar/spectra/am1.5/.
3) Shockley, W.; Queisser, H. J. Detailed Balance Limit of Efficiency of *p-n* Junction Solar Cells. *J. Appl. Phys.* **1961**, *32*, 510–519. doi:10.1063/1.1736034
4) Trotochaud, L.; Mills, T. J.; Boettcher, S. W.; An Optocatalytic Model for Semiconductor–Catalyst Water-splitting Photoelectrodes Based on In Situ Optical Measurements on Operational Catalysts. *J. Phys. Chem. Lett,* **2013,** *4,* 931–935. doi:10.1021/jz4002604